Tomas Bata University in Zlín
Library

Catalytic performance of micro-mesoporous zirconosilicates prepared by non-hydrolytic sol-gel in ethanol-acetaldehyde conversion to butadiene and related reactions

Citation

HRADSKÝ, Dalibor, Petr MACHÁČ, David ŠKODA, Lucie LEONOVÁ, Petr SAZAMA, Jana PASTVOVÁ, Dalibor KAUCKÝ, Dalibor VŠIANSKÝ, Zdeněk MORAVEC, and Aleš STÝSKALÍK. Catalytic performance of micro-mesoporous zirconosilicates prepared by non-hydrolytic sol-gel in ethanol-acetaldehyde conversion to butadiene and related reactions. *Applied Catalysis A: General* [online]. vol. 652, Elsevier, 2023, [cit. 2024-07-02]. ISSN 0926-860X. Available at https://www.sciencedirect.com/science/article/pii/S0926860X23000170

DOI

https://doi.org/10.1016/j.apcata.2023.119037

Permanent link

https://publikace.k.utb.cz/handle/10563/1011378

This document is the Accepted Manuscipt version of the article that can be shared via institutional repository.

TBU Publications
Repository of TBU Publications
publikace.k.utb.cz

Catalytic performance of micro-mesoporous zirconosilicates prepared by non-hydrolytic sol-gel in ethanol-acetaldehyde conversion to butadiene and related reactions

Dalibor Hradsky[a], Petr Machac[a], David Skoda[b], Lucie Leonova[a], Petr Sazama[c], Jana Pastvova[c], Dalibor Kaucky[c], Dalibor Vsiansky[d], Zdenek Moravec[a], Ales Styskalik[a,*]

[a]*Department of Chemistry, Masaryk University, Kotiarska 2, CZ-61137 Brno, Czech Republic*

[b]*Centre of Polymer Systems, Tomas Bata University in Zlin, tr. Tomase Bati 5678, Zlin CZ-76001, Czech Republic*

[c]*J. Heyrovsky Institute of Physical Chemistry, Academy of Sciences of the Czech Republic, Dolejskova 3, CZ-18223 Prague, Czech Republic*

[d]*Department of Geological Sciences, Masaryk University, Kotlarska 2, CZ-61137 Brno, Czech Republic*

[*]*Corresponding author. E-mail address: styskalik@chemi.muni.cz (A. Styskalik).*

ABSTRACT

The open porosity and number of Lewis acid sites in metal silicates ($M = Zr, Ta$) have been reported as key factors enabling reaching high butadiene (BD) productivity from ethanol. However, some microporous zeolites recently displayed very high BD yields. To gain a deeper insight, we have applied non-hydrolytic sol-gel ($NHSG$) in the preparation of micro-mesoporous zirconosilicates. The porosity, structure, and acidity of these materials have been described and compared to a benchmark sample prepared by dry impregnation. The detailed characterization proved that $NHSG$ preparation provided highly homogeneous Zr dispersion in silica leading to almost doubled Lewis acid site numbers and higher activity in ethanol-acetaldehyde conversion to BD, Meerwein-Ponndorf-Verley (MPV) reaction, and aldol condensation, in comparison to the catalyst prepared by dry impregnation. The selectivity and stability were similar for catalysts prepared by $NHSG$ and dry impregnation.

Keywords: Zirconosilicate, micro-mesoporous, non-hydrolytic sol-gel, ethanol to butadiene transformation, aldol condensation, MPV reaction

1. Introduction

The transformation of ethanol to BD (i.e., the ETB process), originally developed at the beginning of the 20th century [**1,2**], has revived in recent years. The possible renewable source of butadiene rubber and related polymers has attracted considerable attention for several reasons. First, naphtha cracking, where BD is produced as a by-product, is a highly energetically demanding process. Second, applying shale gas in the petroleum industry leads to lower BD yields. These facts, together with high oil prices, make the BD a highly demanded product [**3-7**].

The generally agreed mechanism of BD formation from ethanol consists of five steps (**Scheme 1**): (1) ethanol dehydrogenation to acetaldehyde, (2) condensation of two molecules of acetaldehyde to acetaldol, (3) its dehydration to crotonaldehyde, (4) MPV reduction of crotonaldehyde by ethanol to crotyl alcohol with simultaneous production of acetaldehyde, and, finally, (5) dehydration of crotyl alcohol to 1,3-butadiene [**3-8**]. This mechanism was confirmed on Lewis acid $Ta-BEA$ zeolite in a mechanistic study applying in situ $DRIFTS-MS$ setup [**9**]. However, Dussol et al. noted some discrepancies when performing kinetic modeling of ETB process over Ta_2O_5-SiO_2 catalyst and suggested that pathway including intramolecular hydrogen transfer has to be taken into account [**10**].

Catalysts applied in ETB process can be divided into two main groups: (i) catalysts based on mixed magnesia-silica [**11-14**] and (ii) metal silicates and zeolites ($M = Ti, Zr, Hf, Nb, Ta$) [**15-20**]. Dehydrogenation power (first step of the reaction cascade) of both catalyst groups can be improved by introducing Cu, Ag, Ni, usually in the form of metal nanoparticles [**12-14,17**].

To achieve the production of BD from ethanol rentable, catalysts with high productivity and stability are desired. One of the critical factors influencing BD yields over zirconosilicate catalysts has been identified by Sushkevich et al. [**16,17,21**] When comparing $Ag-Zr-BEA$, $Ag-Zr-MCM-41$, and *Ag-ZrO_2-SiO_2* conversion correlated with the number of Lewis acid sites. $Ag-Zr-BEA$ containing isolated zirconium sites displayed the highest activity. Selectivity at iso-conversion remained the same for all three samples [**16**]. The most active $Ag-Zr-BEA$ zeolite catalysts were studied further, and two types of zirconium sites were evidenced: (i) open $Zr(OH)(OSi)_3$ and (ii) closed $Zr\ (OSi)_4$ [**22**]. A linear correlation between the number of open Lewis acid sites and initial BD productivity was established [**21**]. Interestingly, when studying crotonaldehyde MPV reduction by ethanol separately, the authors came to a similar conclusion: initial rates of crotylalcohol production correlated with the number of Lewis acid sites in zirconium-based catalysts [**23**]. Similar, the aldol condensation of butanal performed in a single step over $Zr-BEA$ also depended on the Lewis acid sites, with open Zr sites being more active [**24**].

The effect of porosity on BD productivity and catalyst stability with time-on-stream (TOS) was studied by several groups [**15,18,25**]. Intracrystalline mesoporosity has been introduced into $Zr-BEA$ zeolite by the surfactant-templating method. On the one hand, the stability of both conversion and BD selectivity improved in comparison to the parent microporous $Zr-BEA$ zeolite. On the other hand, conversion and BD selectivity remained at the same levels [**25**]. Chae et al. impregnated *Ta_2O_5* on various silica supports ($SBA-15$, $KIT-6$, etc.) by wet impregnation. The authors showed that the accessibility of active sites is essential as catalysts with larger pores and lower particle sizes performed better in conversion [**15**]. Finally, Dagle et al. impregnated Ag and ZrO_2 on various silica supports and observed that a higher surface area of support provides better Ag dispersion and higher ethanol conversion. On the contrary, BD selectivity decreased with the increasing number of Lewis acid sites as more ethylene was produced [**18**].

The above-discussed findings lead to the conclusion that materials with high Lewis acid site numbers and open porosity (including external) are highly desirable for the ETB process in terms of BD productivity and catalyst stability. In agreement with these results, very high BD productivity (up to 2.18 $gBDgCAT^{h\text{-}1}$) has been reported for highly porous foams with homogeneously dispersed Ta. Moreover, initial BD productivity correlated with the number of Lewis acid sites [**26,27**]. Also accordingly, most catalysts based on zeolites with embedded Zr or Ta excel in conversion and BD selectivity, but suffer from rapid deactivation. Also, the total BD productivity is medium to low (up to 0.60 $gBDgCAT^{h\text{-}1}$) due to limited WHSV used during catalysis over microporous sieves [**6,17,28,29**]. Completely out of these trends are results reported for $Zn-Y-BEA$ catalysts with BD productivities reaching up to 3.6 $gBDgCAT^{h\text{-}1}$ [**30,31**]. The unprecedented BD productivity was ascribed to

confinement effects of micropore channels in BEA zeolite by Dai et al.[**30**]. At the same time, Qi et al. pointed out the enormous activity of $Y(OH)(OSi)_2$ sites closely associated with adjacent silanol groups [**31**].

Herein, we decipher the effect of the number of Lewis acid sites in amorphous micro-mesoporous zirconosilicates prepared by nonhydrolytic sol-gel ($NHSG$) on butadiene production from the ethanol-acetaldehyde mixture, MPV reduction of cyclohexanone, and aldol cross-condensation of benzaldehyde and acetone. Metals promoting ethanol dehydrogenation were not added on purpose to focus on the reactions driven by the acid sites. A benchmark zirconosilicate catalyst was synthesized by dry impregnation, and its Zr distribution was compared to $NHSG-prepared$ samples by numerous characterization techniques. The structural differences are discussed and connected to varying catalytic behavior. The stability of the most active catalyst was studied for 90 h TOS.

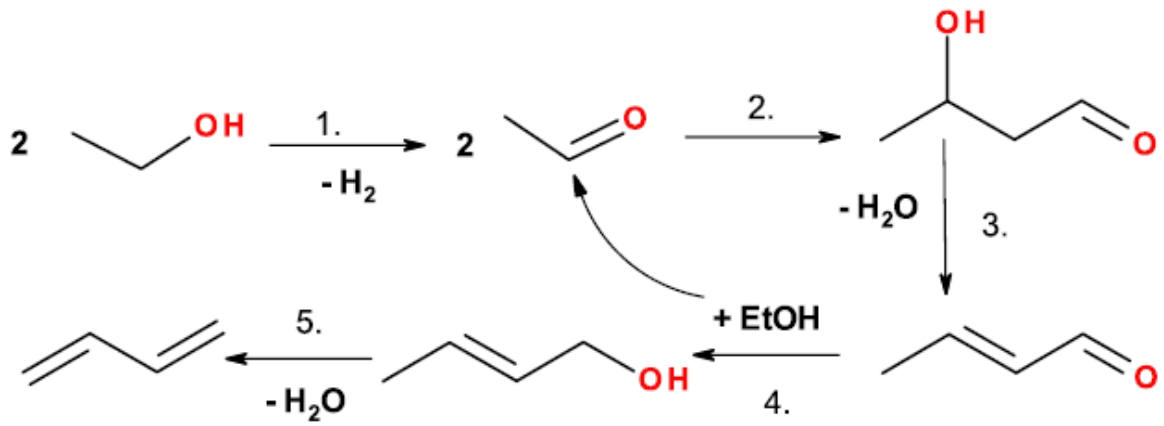

Scheme 1. Mechanism of the direct conversion of ethanol to 1,3-butadiene, according to Toussaint et al. [**8**].

2. Experimental

General experimental methods, characterization techniques, and spectroscopic characterization data (IR) can be found in the supporting material of this manuscript.

2.1. Xerogel synthesis - acetamide/acetic anhydride elimination route

Silicon tetraacetate (8.269 g, 31.29 mmol) was loaded in an autoclave in a glove box and dissolved in 40 cm^3 CH_2Cl_2. Additionally, tri-methylsilylated Pluronic F127 (4.015 g) was added and dissolved in the solution of silicon tetraacetate. In a separate vial, $Zr(NEt_2)_4$ (0.186 g, 0.490 mmol) was dissolved in toluene (10 cm^3) and stirred at RT for 5 min. The solution of $Zr(NEt_2)_4$ in toluene was then added to the solution of silicon tetraacetate and trimethylsilylated Pluronic F127 in dichloromethane under vigorous stirring (5 min). The autoclave was sealed and kept in an oven at 160 °C for 72 h. During this time, gelation occurred. After cooling down, the autoclave was put back into the glo-vebox, opened, and the gel was transferred into a Schlenk vessel. The gel was then dried under a vacuum at 60 °C overnight to remove the solvent and volatile condensation products (N, N'-diethylacetamide and acetic anhydride). The resulting powder was calcined in an ambient air atmosphere at 500 °C (5 °C min^{-1}, 5 h), yielding a bright white catalyst (**NH-160**; NH stands for non-hydrolytic, 160 stands for the temperature used during gelation) with a nominal molar Si/Zr ratio 63.9 (**Table 1, Scheme 2**).

2.2. Xerogel synthesis - acetamide/acetyl chloride elimination route

Silicon tetraacetate (4.333 g, 16.40 mmol) was loaded in an autoclave in a glove box and dissolved in 40 cm^3 CH_2Cl_2. Silicon tetrachloride (2.695 g, 15.86 mmol) and trimethylsilylated Pluronic F127 (2.000 g) were added to the solution of silicon tetraacetate, forming a clear solution. In a separate vial, $Zr(NEt_2)_4$ (0.193 g, 0.508 mmol) was dissolved in toluene (10 cm^3) and stirred at RT for 5 min. The solution of $Zr(NEt_2)_4$ in toluene was then added to the solution of silicon tetraacetate, silicon tetrachloride, and Pluronic F127 in dichloro-methane under vigorous stirring (5 min).

Table 1 Synthesis, XPS, and $ICP-OES$ data for $NHSG-made$ zirconosilicate catalysts.

Sample	n Si $(OAc)_4$ (mmol)	n $SiCl_4$ (mmol)	n Zr $(NEt_2)_4$ (mmol)	Si/Zr ratio (-) Theor/ICP/XPS
NH-160	31.29	–	0.490	63.9/76.5/106
NH-140	16.40	15.96	0.508	63.7/64.3/93
DI-140	16.40	15.86	0.058	51.3[a]/58.3/42

[a] *The rest of Zr to achieve the desired ratio was introduced by dry impregnation of $ZrO(NO_3)_2$ on the sample.*

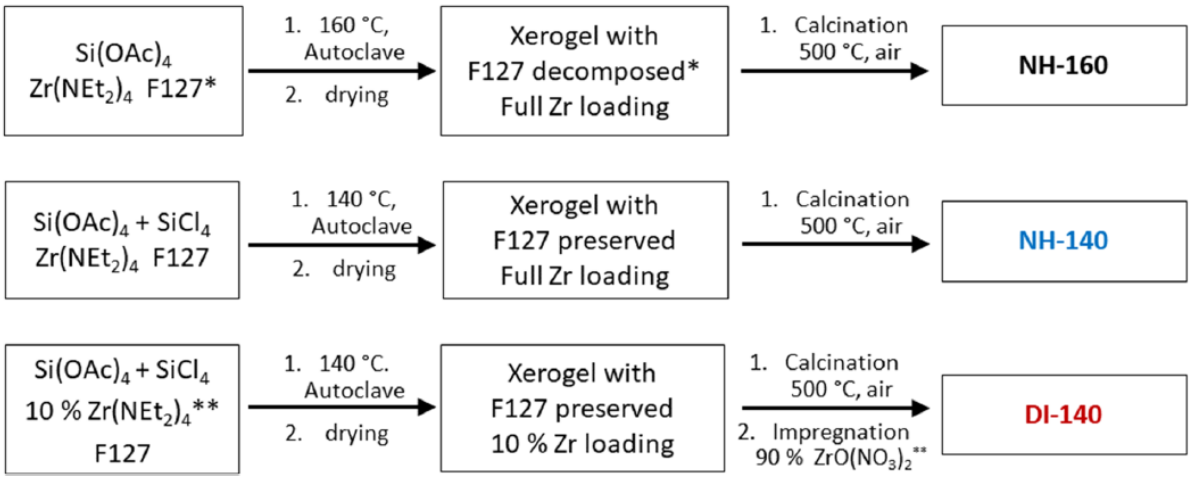

Scheme 2. The preparation scheme of the zirconosilicate catalysts. *The decomposition of Pluronic F127 has been observed after the sol-gel reaction at 160 °C (e.g., ethylene glycol diacetate observed in $GC-MS$ of volatiles) in contrary to the sol-gel reactions performed at 140 °C. **Only 10 mol% of total Zr has been added to the reaction mixture to enhance the condensation reaction. The rest 90 mol% was dry-impregnated to prepare a benchmark catalyst with similar porosity, but applying a conventional method of Zr deposition.

The autoclave was sealed and kept in an oven at 140 °C for 72 h. During this time, gelation occurred. After cooling down, the autoclave was put back into the glovebox, opened, and the gel was transferred into a Schlenk vessel. The gel was then dried under vacuum at 60 ° C overnight to remove the solvent and volatile condensation products (N, N'-diethylacetamide and acetyl chloride). The resulting powder was calcined in an ambient air atmosphere at 500 °C (5 °C min^{-1}, 5 h), yielding a bright white catalyst (NH-140; 140 stands for the temperature used during gelation) with a nominal molar Si/Zr ratio 63.7 (**Table 1, Scheme 2**). For comparison, zirconosilicate with nominal molar Si/Zr ratio 556 (0.022 g,

0.058 mmol $Zr(NEt_2)_4$ was prepared following the same experimental procedure and used as a support for zirconyl nitrate dry impregnation providing sample DI-140 (DI stands for dry impregnation) exhibiting similar Si/Zr ratio to samples prepared in one-step by $NHSG$ (**Table 1, Scheme 2**).

2.3. Dry impregnation

Sample prepared by $NHSG$ (1.558 g) with nominal molar Si/Zr ratio 556 was mixed with a solution of hydrated $ZrO(NO_3)_2$ (0.103 g, 0.335 mmol) in water (2 cm^3), forming a white paste. The paste was dried in an oven at 130 °C for two hours and then calcined in an ambient air atmosphere at 500 °C (5 °C min^{-1}, 5 h), yielding a bright white catalyst (***DI*-140**) with a nominal molar Si/Zr ratio 51.3 (**Table 1, Scheme 2**).

2.4. Ethanol-acetaldehyde mixture conversion to butadiene

The calcined xerogel catalysts (0.100 g, sieved in the 0.20-0.40 mm particle size range) were diluted with glass beads (0.5-1 mm) to keep the volume of the catalyst bed constant. The void space of the reactor was filled with silica beads. Catalytic testing was carried out by injecting 0.065 g h^{-1} of a mixture of absolute ethanol/acetaldehyde (2.5 molar ratio) using NE-300 syringe pump in a 50 cm^3 min^{-1} flow of N_2. The tests were carried out at atmospheric pressure, $WHSV = 0.65$ h^{-1}. The temperature was varied stepwise (255, 290, and 325 °C). One step consisted of (i) a heating ramp (5 °C min^{-1}) and stabilization at the set temperature (21 min) and (ii) a steady temperature state (120 min). The analysis of the effluent gas was carried out by a HP 6890 Gas Chromatograph (at least 10 injections at each temperature) equipped with a flame ionization detector (FID) and a TG-BOND U column (30 m long, internal diameter 0.32 mm, film thickness 10 μm). The preliminary stability of the catalysts was tested by maintaining the highest temperature (325 °C) for 14 h. The stability of catalytic performance of sample NH-140 was tested for 90 h TOS at 325 °C.

2.5. MPV reduction of cyclohexanone by isopropanol

A suspension of zirconosilicate catalyst (dried at 150 °C under vacuum for 1 h, 0.0213 mmol Zr) in dry isopropanol (15 cm^3) was prepared. Cyclohexanone (0.3182 g, 3.240 mmol) and nonane (0.0718 g, 0.560 mmol) were added, and the reaction mixture was refluxed for 4 h under reflux condenser (oil bath temperature 115 °C). Aliquots for $GC-MS$ analysis were withdrawn every hour and prepared by filtration via 0.22 pm $PTFE$ syringe filter.

2.6. Acetone-benzaldehyde aldol cross-condensation

A suspension of zirconosilicate catalyst (dried at 150 °C under vacuum for 1 h, 0.0168 mmol Zr) in dry toluene (10 cm^3) was prepared. Benzaldehyde (0.0891 g, 0.840 mmol), acetone (0.1464 g, 2.521 mmol), and nonane (0.0718 g, 0.560 mmol) were added, and the reaction mixture was kept at 90 °C for 4 h under reflux condenser. Aliquots for $GC-MS$ analysis were withdrawn every hour and prepared by filtration via 0.22 pm $PTFE$ syringe filter.

3. Results and discussion

3.1. Synthesis

Zirconosilicate samples were prepared by $NHSG$, a technique known to produce mixed metal oxides with high homogeneity of metal mixing and good textural properties[**32-37**]. Particularly, herein we present further development of our previous work on non-hydrolytic sol-gel condensation between silicon tetraacetate and zirconium tetrakis (diethylamide) providing zirconosilicate catalysts [**38**]. While zircono-silicates in 1:1 $Si{:}\,Zr$ molar ratio have already been prepared before (Schlenk vessel, toluene, 80 °C) [**38**], here we report the reaction conditions enabling the $Si{:}\,Zr$ molar ratio increase to 64:1 to modulate the catalysts' acidity.

Two novel variations of the acetamide elimination route[**38-41**] were studied. In the first of them, the zirconium diethylamide was mixed with silicon tetraacetate in a 1:64 ratio, and the mixture was heated to 160 °C in an autoclave to induce condensation reactions (**Eq**. (**1**); **Scheme 2**; sample $\boldsymbol{NH}$**-160**). In the second one, the temperature necessary to obtain a gel was lowered thanks to the application of $SiCl_4$ (**Eq**. (**2**); **Scheme 2**; sample **NH-140**). Silicon tetrachloride reacted more promptly with silicon tetraacetate forming acetyl chloride and $Si{-}O{-}Si$ bridges (**Eq**. **2**) compared to the self-condensation of acetoxy groups forming acetic anhydride (**Eq**. (**1**)).

$$Zr(NEt_2)_4 + 64\ Si(OAc)_4 \rightarrow ZrO_2{\bullet}64SiO_2 + 4\ AcNMe_2 + 126\ AcOAc \quad (1)$$

$$Zr(NEt_2)_4 + 31{\cdot}5\ SiCl_4 + 32{\cdot}5\ Si(OAc)_4 \rightarrow ZrO_2{\bullet}64SiO_2 + 4\ AcNMe_2 + 126\ AcCl \quad (2)$$

The second variety of the acetamide elimination route (**Eq**. (**2**)) was applied to prepare a benchmark sample (**Scheme 2**): The synthesis was performed with only 10 % of total Zr content (metals are necessary to induce the condensation reactions) [**42,43**]. The rest of Zr (i.e., ca. 90 %) was introduced by dry impregnation of hydrated zirconyl nitrate (sample $\boldsymbol{DI-140}$). In such a way, the benchmark sample with zirconium introduced by a common and simple method exhibited similar porosity to the samples prepared by $NHSG$ in one step (see below).

The nominal $Si{:}\,Zr$ ratio was 64 in $NHSG$-prepared zirconosilicates. $ICP-OES$ analysis confirmed that applied synthetic strategies provide samples with Si:Zr ratios close to the nominal values (**Table 1**). The surface composition was analyzed by XPS, and the Si/Zr ratio was calculated (**Table 1**). For the catalysts where the zirconium was incorporated through non-hydrolytic sol-gel ($\boldsymbol{NH-160}$ and $\boldsymbol{NH-140}$), the experimental surface Si/Zr molar ratio was higher than the nominal value (64), similarly to some previously reported $NHSG$-prepared met-allosilicates [**44**]. On the contrary, when zirconium was incorporated by impregnation ($\boldsymbol{DI-140}$), the Si/Zr surface molar ratio reached 42, indicating a higher amount of zirconium on the catalyst surface as expected.

Pluronic F127 as a pore-generating agent was added in all $NHSG$ reaction mixtures, similar to previously published reports applying the acetamide elimination route [**38,39,45**]. However, in the first

reaction (**Eq. 1**, higher temperature, 160 °C), it was observed, that Pluronic is not stable under the given reaction conditions and is cut to its monomer fragments (e.g., ethylene glycol diacetate observed in $GC-MS$ of volatiles; **Scheme 2**). It can be deemed probable that Pluronic depolymerization was catalyzed by Zr sites as the monomer Pluronic fragments were not observed at similar reaction conditions (160 °C, autoclave, dichloromethane) applied for the synthesis of aluminosilicate catalysts [**46**]. Fragmented Pluronic partially lost its ability to work as a pore-generating agent, and a sample with a broad pore size distribution ($\boldsymbol{NH-160}$) was obtained (see Section 3.2 Porosity). On the contrary, the lower temperature used for the second reaction (140 °C, **Eq. 2**) prevented Pluronic from splitting, and samples $\boldsymbol{NH-140}$ and DI-140 exhibited isotherms typical for $NHSG$-prepared samples in the presence of Pluronic (see **Section 3.2** Porosity) [**38,39,45**].

3.2. Porosity

N_2 adsorption-desorption isotherms are shown in **Fig. 1**A. The preparation at 160 ° C induced Pluronic F127 decomposition (see **Scheme 2** and **Section 3.1**) and produced sample $\boldsymbol{NH-160}$ represented by isotherm without any apparent hysteresis, though increasing in the whole pressure range. On the other hand, the samples prepared at a lower temperature ($\boldsymbol{NH-140}$ and $\boldsymbol{DI-140}$) are represented by Type IV isotherms with hysteresis in the medium pressure range, indicating the presence of relatively uniform mesopores. The difference between samples prepared at 140 and 160 °C was observed in the pore size distribution: Sample $\boldsymbol{NH-160}$ exhibited similar but broader pore size distribution in comparison to $\boldsymbol{NH-140}$ and $\boldsymbol{DI-140}$ (**Fig. 1**B).

The SA_{BET}, V_{total}, V_{micro}, Vmeso, and D for all samples are summarized in **Table 2**. Samples $\boldsymbol{NH-160}$ and $\boldsymbol{NH-140}$ displayed a higher specific surface area than $\boldsymbol{DI-140}$. The pore volumes were quite similar for all samples ranging from 0.52 to 0.66 $cm^3\ g^{-1}$. Pore size distribution maxima reached 3.7 nm for all samples. The volume fraction represented by micropores was also similar (11-26 %) and therefore all samples can be described as micro-mesoporous zirconosilicates. The only significant difference among the samples regarding porosity thus remained the missing hysteresis in the case of $\boldsymbol{NH-160}$ and its broader pore size distribution which can be related to Pluronic F127 decomposition.

3.3. Zr dispersion in zirconosilicates

IR, XPS, and $DRUV-Vis$ spectroscopy and XRD were applied to describe the structure of the samples and especially the Zr dispersion. $X-ray$ diffractograms (**Fig. 2**A) showed mostly amorphous character with a broad maximum at ca. 27°2θ. While zirconosilicates prepared by $NHSG$ were completely amorphous, sample $\boldsymbol{DI-140}$ displayed very weak diffractions (asterisks in **Fig. 2**A). These diffractions fitted well with the ICSD#99744 card suggesting presence of traces of tetragonal zirconia phase detectable by the XRD analysis and thus a lower zirconium dispersion within the sample prepared by dry impregnation.

Table 2 Textural properties of $NHSG$-prepared samples.

Sample	SA_{BET} ($m^2\ g^{-1}$)	V_{total}[a] ($cm^3\ g^{-1}$)	V_{micro}[b] ($cm^3\ g^{-1}$)	V_{meso}[b] ($cm^3\ g^{-1}$)	V_{micro}[b] (%)	D[c] (nm)
NH-160	710	0.66	0.07	0.59	11	3.7
NH-140	790	0.54	0.14	0.40	26	3.7
DI-140	630	0.52	0.09	0.43	17	3.7

[a] *Estimated at* $P/Po\ = 0.97$.

[b] *based on* t*-plot analysis.*

[c] *Maxima observed in* $NLDFT$ *pore size distributions.*

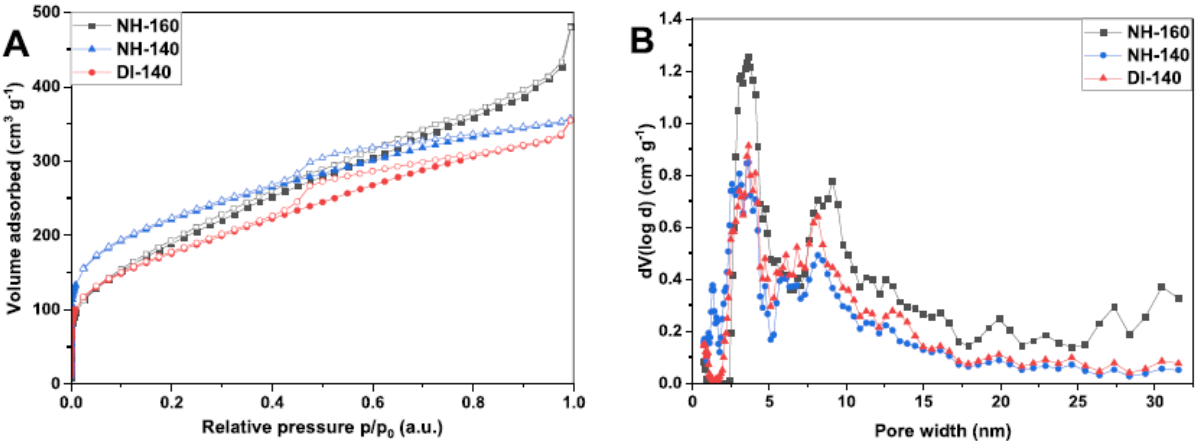

Fig. 1. N_2 adsorption desorption isotherms of $NHSG$-prepared zirconosilicate samples (left) and $NLDFT$ pore size distributions (right).

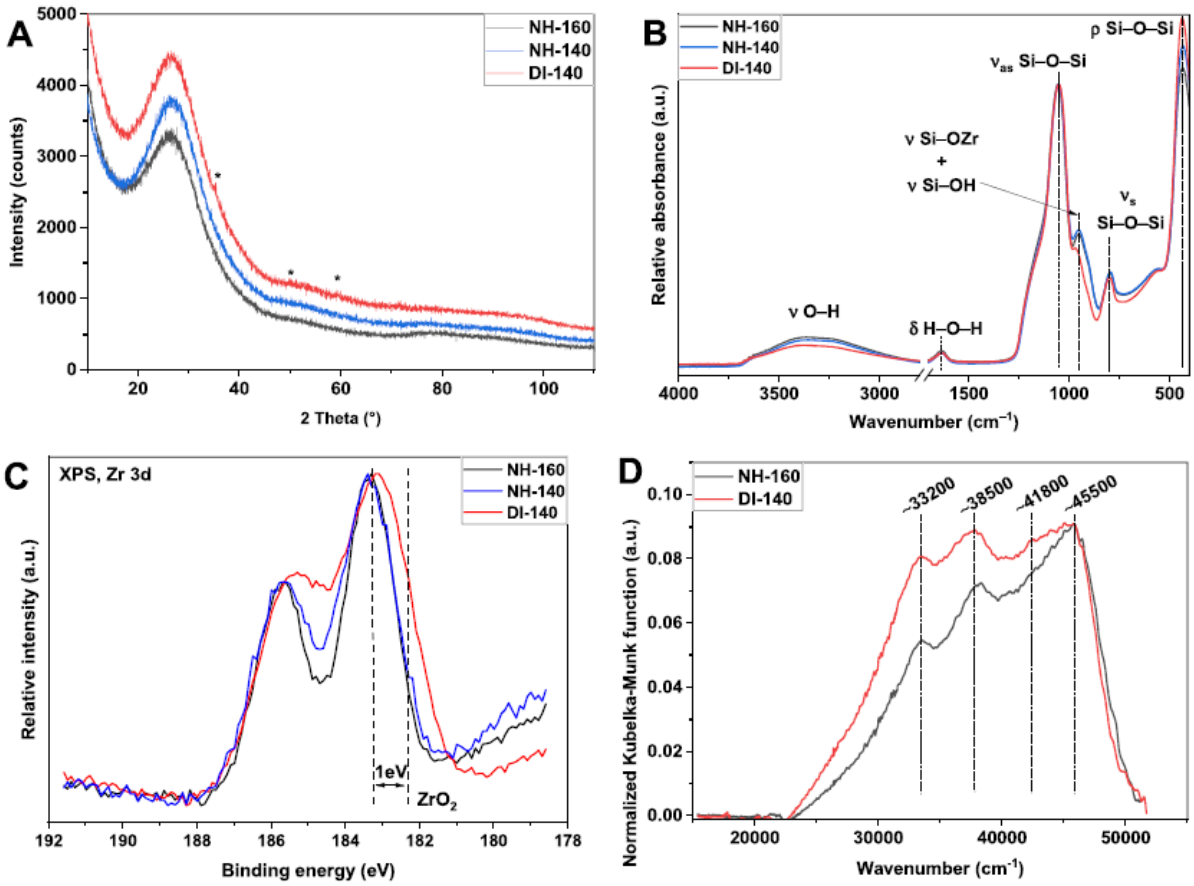

Fig. 2. $X-ray$ diffractograms (A), IR (B), XPS (C),

IR spectra were very similar for all three samples (**Fig. 2**B). The zirconosilicates exhibited absorption bands at 1055- 1049 cm^{-1} (vas $Si—O—Si$), 794- 798 (vs $Si—O—Si$), and 430 cm^{-1} (p $Si—O—Si$) typical for silica-based samples. Furthermore, absorption bands at 1634 cm^{-1} (5 $H—O—H$) and 3000-3600 cm^{-1} (v O—H, broad) originating from adsorbed water and surface silanol groups were present. Notably, the band of medium intensity at 954- 965 cm^{-1} was observed which might originate both in $Si—OZr$ and $Si—OH$ stretching vibration [**19,47,48**]. The intensity of this band was shown to correlate with the number of $Si—O—Zr$ bridges [**38,49,50**] and thus can be used to estimate the homogeneity of the Zr dispersion in zirconosilicates. A higher intensity was observed for samples $\boldsymbol{NH-140}$ and $\boldsymbol{NH-160}$ compared to $\boldsymbol{DI-140}$, indicating a better Zr dispersion in $NHSG-prepared$ samples in agreement with XRD measurements (assuming a similar $Si—OH$ groups content).

$X-ray$ photoelectron spectroscopy and especially Zr 3d peak was analyzed to further assess the zirconium atoms dispersion (**Fig. 2**C). While $NHSG$ prepared samples ($\boldsymbol{NH-160}$ and $\boldsymbol{NH-140}$) display narrow and well-resolved peaks ($FWHM$ reached 1.8 and 1.6 eV, respectively), the $\boldsymbol{DI-140}$ is represented by a broader and poorly resolved signal (FWHM 4.1 eV) shifted to a lower binding energy. According to the literature, the binding energy for Zr in ZrO_2 lies in the range from 182.2 to 182.6 eV [**51**]. Zr incorporated in BEA zeolite is shifted to higher binding energy by 0.7-1.0 eV due to a higher electronegativity of Si in comparison to Zr [**16,23,52**]. The shift of Zr 3d peak to higher binding energy was also observed in crystalline $ZrSiO_4$ [**53**]. A similar trend was observed for Ti and Ta dispersed in silica and explained by a lower electron density of metals once incorporated in silica compared to their respective metal oxides and, thus, higher binding energy [**41,54**]. Based on these

reports, it can be inferred that a shift to lower binding energies for sample $\boldsymbol{DI-140}$ can be explained by a formation of poorly dispersed ZrO2 particles on the silica surface. On the contrary, samples prepared by $NHSG$ ($\boldsymbol{NH-160}$ and $\boldsymbol{NH-140}$) exhibit similar binding energies to $Zr-BEA$ and crystalline $ZrSiO_4$, indicating a homogeneous dispersion of Zr in silica matrices. These results agree with conclusions based on the XRD and IR spectroscopy.

$DRUV-Vis$ spectroscopy was also applied to compare the zirconium dispersion in samples prepared by $NHSG$ and dry impregnation ($\boldsymbol{NH-160}$ and $\boldsymbol{DI-140}$; **Fig. 2**D). Four absorption maxima were observed in both zirconosilicates at ca. 45500, 41800, 38500, and 33200 cm^{-1}. While the absorption maximum at the highest wavenumber (45500 cm^{-1}, i.e., 220 nm) corresponds to ligand-to-metal charge transfer ($LMCT$) in $Zr—O—Si$ bridges in four-coordinated Zr, the maxima at lower wavenumbers come from the Zr species with increasing coordination numbers in zirconia clusters containing a higher content of $Zr—O—Zr$ linkages [**55,56**]. In accordance with the previous results (IR and XPS spectroscopy, XRD) the maximum intensity for the band at 45500 cm^{-1} was observed in **NH-160**, and the amplitude of bands of lower wavenumbers was decreasing (**Fig. 2**D, Fig. 1S). In sample $\boldsymbol{DI-140}$ all bands reached similar intensities (not decreasing contrary to $\boldsymbol{NH-160}$), indicating a higher content of zirconia clusters (**Fig. 2**D, Fig. 2S). These results confirm a more homogeneous Zr dispersion in $\boldsymbol{NH-160}$ in comparison to $\boldsymbol{DI-140}$.

The scanning transmission electron microscopy combined with the energy-dispersive spectroscopy ($STEM-EDS$) was applied to further study the Zr dispersion in $\boldsymbol{NH-160}$, $\boldsymbol{NH-140}$, and $\boldsymbol{DI-140}$ (**Fig. 3** and 3S). While the Si, O, and Zr elemental maps for $NHSG$-prepared samples overlap and show homogeneously distributed Zr, the micrographs recorded for DI-140 displayed clear and marked differences in Zr content among the catalyst particles. Thus, the $STEM-EDS$ analysis agrees well with results observed in IR, XPS, and $DRUV-Vis$ spectra, and XRD.

The Zr incorporation was further studied by NMR analyses. ^{29}Si $CPMAS\ NMR$ spectra (Fig. 4S) were very similar for $\boldsymbol{NH-160}$, $\boldsymbol{NH-140}$, and $\boldsymbol{DI-140}$.

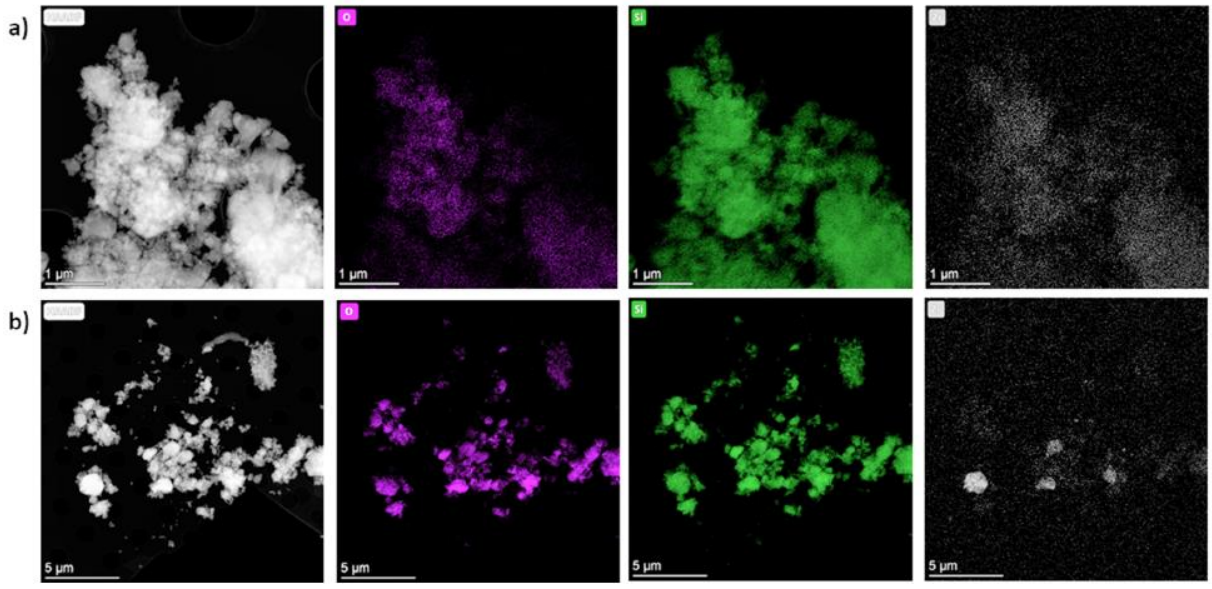

Fig. 3. $STEM-EDS$ elemental maps of samples $NH-140$ (a) and $DI-140$ (b). Color code: Violet - O, green - Si, and grey - Zr.

Three signals at — 91, — 100, and — 110 ppm were observed in all three samples representing $Si(OSi)_2(OX)_2$, $Si(OSi)_3(OX)$, and $Si(OSi)_4$, species, respectively ($X = H$ or Zr) [**38**]. No significant difference was observed, probably due to a relatively low Zr loading in zirconosilicate samples.

Chemisorbing triethylphosphine oxide ($TEPO$) on zirconosilicate samples and collecting $^{31}P\ MAS\ NMR$ spectra was used to further understand the Zr dispersion and get a preliminary insight into the acid site quality (**Fig. 4**) [**57-59**]. Two major signals at 66 and 74 ppm and one minor peak at 101 ppm were observed in all three samples, probably representing three different acid sites. The chemical shift of observed chemisorbed species can be used to compare the acid site strength: the more downfield (i.e., higher chemical shift) the signals appear, the stronger the interaction between $TEPO$ and the acid site [**57**].

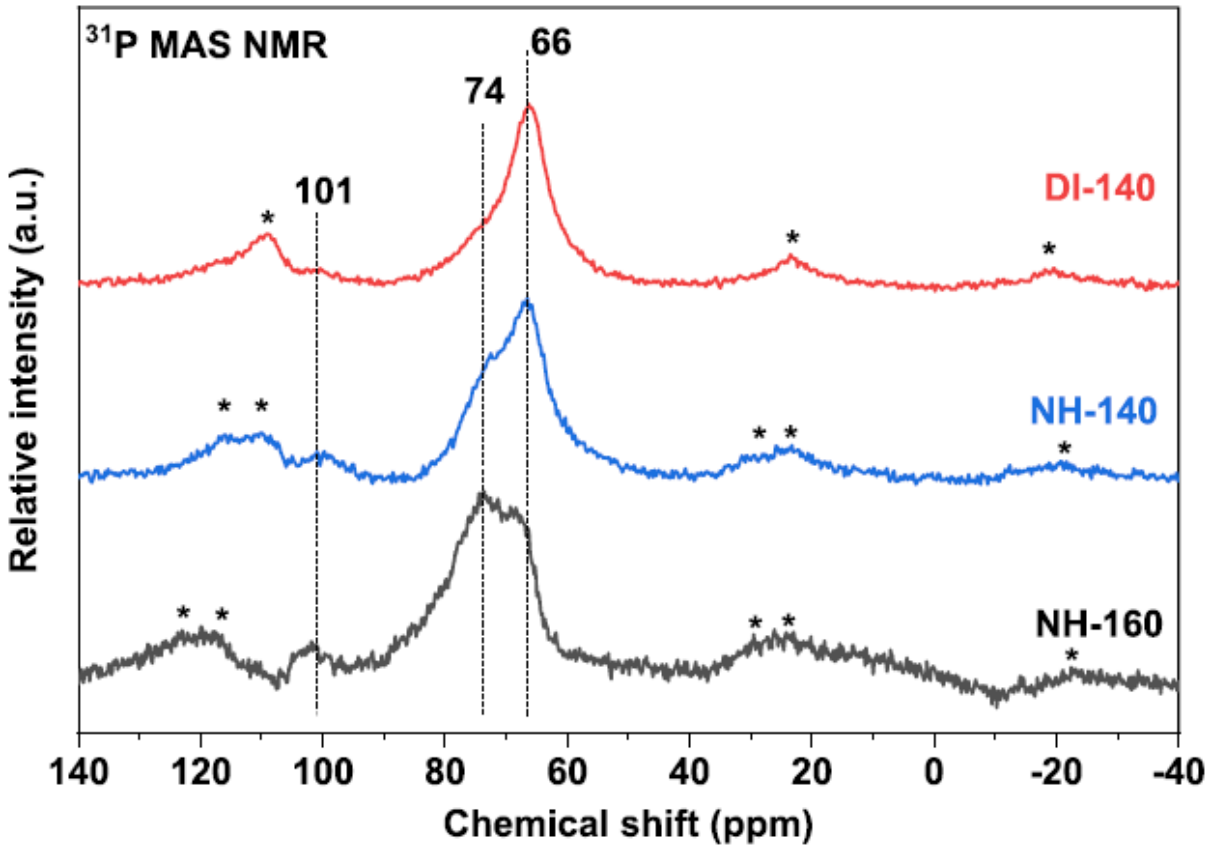

Fig. 4. $31P\ MAS\ NMR$ spectra collected after triethylphosphine oxide chemisorption on zirconosilicate samples. Asterisks denote spinning sidebands.

Comparing the spectra of $\boldsymbol{NH-160}$ and $\boldsymbol{NH-140}$ with $\boldsymbol{DI-140}$, it can be concluded that $NHSG$-prepared samples contained significantly more stronger acid sites (signal at 74 ppm) than sample prepared by dry impregnation, governed by a peak at 66 ppm. These two major signals represent acid sites of medium strength [**57**]. The minor peak at 101 ppm (strong interaction between the acid site and $TEPO$) [**57,58**] exhibits only a low intensity. Still, it seems to be present in higher quantities in $NHSG$ samples compared to $\boldsymbol{DI-140}$.

Noteworthy, a similar pattern to NHSG-prepared zirconosilicates was observed in $^{31}P\ NMR$ spectra of trimethylphosphine oxide ($TMPO$) chemisorbed on $Sn-, Zr$-, and $Hf-BEA$ zeolites (i.e., two main signals shifted downfield from physisorbed $TMPO$ by ca. 14 and 18 ppm, respectively) [**59**]. In $\boldsymbol{NH-160}$ and $\boldsymbol{NH-140}$ the two main chemisorbed TEPO signals were shifted downfield by ca. 14 and 22 ppm from physisorbed $TEPO$ molecules (~52 ppm), respectively [**58**]. On the contrary, $TMPO$

adsorbed on $Si-BEA$ zeolite decorated with SnO_2 particles showed only a broad resonance representing physisorbed $TMPO$ molecules. Thus, TMPO adsorption unambiguously distinguished metal oxide particles supported on zeolite from the well-dispersed Lewis acid sites (Sn, Zr, Hf) in zeolite matrices [**59**]. Therefore, the $^{31}P\ NMR$ spectra of adsorbed $TEPO$ species confirm the homogeneous Zr dispersion in $NHSG-prepared$ samples and the formation of three different acid sites with medium (66 and 74 ppm) to strong (101 ppm) acid site strength.

3.4. Acid sites characterization

The amount, nature, and strength of acid sites were determined by pyridine adsorption followed by $FTIR$ analysis (**Fig. 5**A-D and **Table 3**). The $FTIR$ spectra of adsorbed pyridine revealed the presence of an intensive absorption band at 1445 cm^{-1} and a barely visible absorption band at 1545 cm^{-1} attributed to pyridine interaction with the Lewis and Brpnsted acid sites, respectively (**Fig. 5**A-C). Mostly Lewis acid sites are present in the samples. Their total amount was determined by integrating the intensity of the absorption band at 1455 cm^{-1}; the molar extinction coefficient according to Emeis [**60**] was used in calculations. A presence of a negligible amount of Brpnsted acid sites in the samples is questionable similar to other zirconosilicate materials [**18-20,24,52**]. The characteristic band at 1545 cm^{-1} displays a very weak intensity, similar to rotational bands of water vapor present in the chamber of the IR instrument. Eventually, OH groups in zirconosilicates have been reported as too weak to protonate pyridine [**18**]. The clear-cut answer regarding Brpnsted acid sites could not be obtained from 3300- 3800 cm^{-1} region either (**Fig. 5**D). While the presence of a broad absorption band between 3400 and 3700 cm^{-1} could be explained as an indication of Brpnsted acid sites [**61**], it might also originate from the presence of remaining water that was not completely desorbed under the degassing conditions.

Table 3 Amount and strength of Lewis acid sites in $NHSG$-prepared zirconosilicates and benchmark catalyst prepared by dry impregnation estimated by pyridine adsorption combined with IR spectroscopy (spectra used to obtain these

Sample	Total acid sites (mmol g^{-1})	Acid sites after desorption at 150 °C (%)	Acid sites after desorption at 250 °C (%)
NH-160	0.063	62	23
NH-140	0.085	74	13
DI-140	0.044	69	11

The presence of non-completely desorbed water molecules could be further corroborated by a broad absorption band at 1640 cm^{-1} arising from deformation vibration in H_2O (**Fig. 5**A-C). Therefore, the existence of Brpnsted acid sites in the zirconosilicate catalysts can not be unambiguously confirmed.

The strength of Lewis acid sites was approached by looking at a fraction of sites that were preserved after degassing at 150, 250, and 350 °C (**Table 3**). The analysis of pyridine desorption shows that NHSG-prepared catalysts $\boldsymbol{NH-160}$ a $\boldsymbol{NH-140}$ and the DI-140 sample possess weak and medium-strength Lewis acid sites (pyridine mostly desorbed at 250 °C; no pyridine after evacuation at 350 °C). The fractions of sites preserved after degassing at 150 °C and 250 °C are very similar among the samples (62-74 % and 11-23 %, respectively), indicating similar strength distribution of the acid sites.

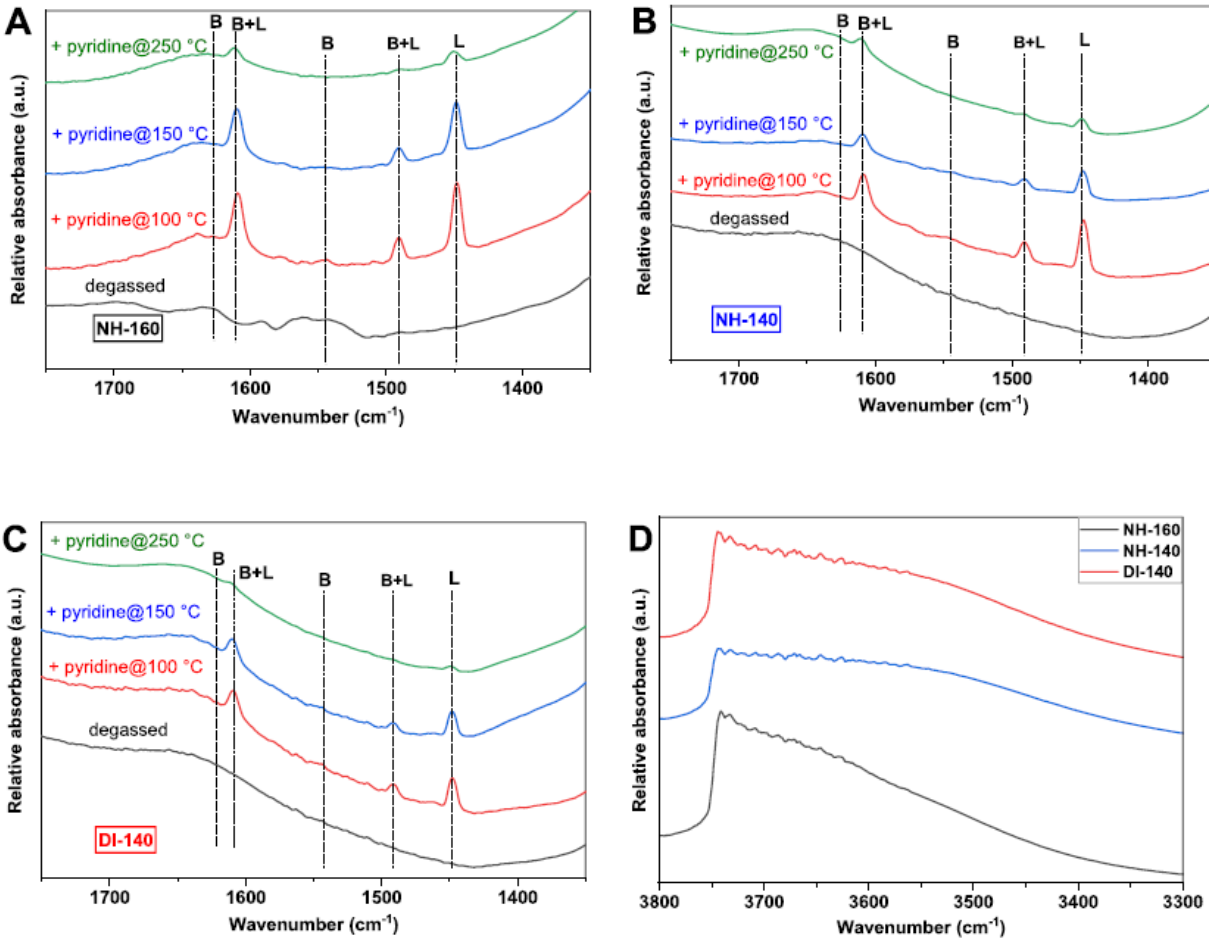

Fig. 5. IR spectra of $NH-160$ (A), $NH-140$ (B), and $DI-140$ (C), degassed, and after pyridine adsorption and degassed at different temperatures. IR spectra of OH region of all three degassed samples (D). A quantitative analysis of the data is presented in **Table 3**.

The most apparent difference between the samples was observed in the acid site numbers. The total amount of acid sites in the studied catalysts varied from 0.044 to 0.085 mmol g^{-1} (**Table 3**), with $\boldsymbol{DI-140}$ containing the lowest number of acid sites and $\boldsymbol{NH-140}$ reaching the highest acid site number. These values found for the different samples support the findings of previously described methods (IR, XPS, and $DRUV-Vis$ spectroscopy, $STEM-EDS$, XRD): Samples with homogeneous Zr distribution ($\boldsymbol{NH-160}$ and $\boldsymbol{NH-140}$) feature higher acid site numbers than $\boldsymbol{DI-140}$ containing poorly dispersed Zr, though $\boldsymbol{DI-140}$ displays a higher Zr bulk and surface concentration ($ICP-OES$, XPS, **Table 1**). The slightly higher concentration of the Lewis acid centers in the $\boldsymbol{NH-140}$ sample compared to $\boldsymbol{NH-160}$ is consistent with the slightly higher concentration of Zr in the $\boldsymbol{NH-140}$ sample (**Table 1**).

Recently, the influence of acid site quality in heterogeneous catalysis has been thoroughly discussed, particularly the open and closed acid sites in the case of $Zr-BEA$ zeolites [**21,24,59**]. Here, we have observed mostly Lewis acid sites with similar strength according to the pyridine adsorption followed by $FTIR$ analysis. However, $^{31}P\ NMR$ spectroscopy of chemisorbed $TEPO$ suggested some differences in acid site quality: $NHSG-prepared$ samples contained more stronger acid sites. Despite the similarities between the $^{31}P\ NMR$ spectra obtained here and by Lewis on $Zr-BEA$ zeolites with adsorbed $TMPO$ [**59**], it is impossible to give a more precise and clear-cut answer regarding the acid sites quality in zirco-nosilicates presented herein due to the lack of literature data. Therefore, in the

following discussion on catalytic properties, we will stick to the data gained from pyridine adsorption followed by $FTIR$ analysis.

3.5. MPV redox reaction and aldol condensation in batch

Two catalytic experiments in the liquid phase in batch connected to the ETB process were performed with all three zirconosilicate samples: (i) MPV redox reaction and (ii) aldol condensation. Either the former or the latter reaction has been reported as the rate-limiting step of the ETB process (Step 2 and 4, **Scheme 1**) in various mechanistic and kinetic studies [**4**]. The dehydration reactions (Step 3 and 5, **Scheme 1**) are easily achieved at the reaction conditions used in the ETB process (T = 325-425 °C) [**4**]. Therefore, we decided to study MPV redox reaction and aldol condensation individually and in more detail. However, different substrates have been chosen to work at lower temperatures, in the liquid phase, batch.

First, cyclohexanone was reacted with isopropanol providing cyclo-hexanol and acetone (MPV redox reaction; **Scheme 3**) [**38,52,62**]. No other products were observed. Thus the cyclohexanol yields (**Fig. 6**A) followed the cyclohexanone conversions. The activity in the performed reaction followed the number of Lewis acid sites: $\boldsymbol{NH-140 > NH-160 > DI-140}$. These results are in good agreement with Sushkevich et al., [**23**] who studied the MPV reduction of crotonalde-hyde with ethanol over Zr-containing catalysts. The authors concluded that the initial crotyl alcohol formation rates followed the Lewis acid site numbers. Similarly, Zhu et al. reported much higher activity for well-dispersed Lewis acid Zr sites in $Zr-BEA$ zeolite in cyclohexanone and tert-butylcyclohexanone reduction by isopropanol in comparison to the supported ZrO_2 catalysts [**52**]. The materials presented herein showed much lower catalytic activities than exhibited by $Zr-BEA$ zeolites at similar conditions (19.3 % cyclohexanone conversion after 4 h vs. 94.5 % after 30 min exhibited by $\boldsymbol{NH-140}$ and $Zr-BEA$ zeolite with Si:

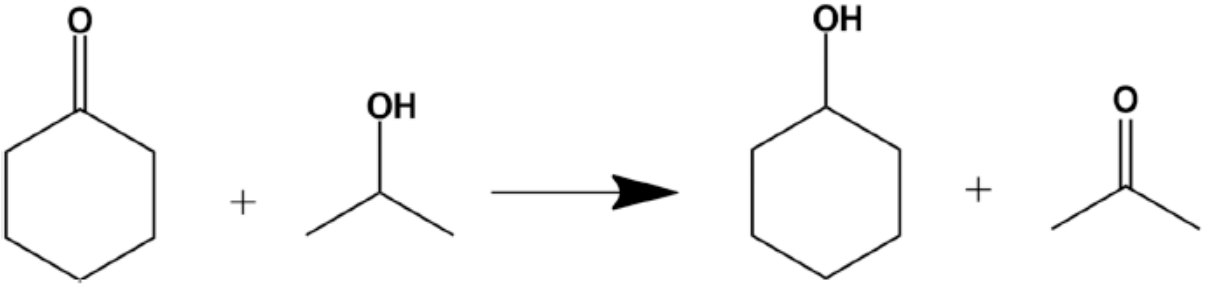

Scheme 3. MPV reduction of cyclohexanone with isopropanol.

Zr ratio equal to 100, respectively) [**52**]. Zirconosilicate catalysts $\boldsymbol{NH-140}$, $\boldsymbol{NH-160}$, and $\boldsymbol{DI-140}$ showed comparable cyclohexanone conversions to mostly amorphous zirconosilicates-$Zr-BEA$ zeolites (42-89 % conversion after 5 h) [**62**].

Similar results were obtained for aldol cross-condensation of benz-aldehyde with acetone (**Scheme 4**). This reaction provided benzalace-tone solely. Thus, the conversion and benzalacetone yield were equal (**Fig. 6**B). Similar to MPV redox reaction, the activity followed the Lewis acid site numbers: $\boldsymbol{NH-140 > NH-160 > DI-140.}$ This finding agrees well with Ordomsky et al., who confirmed the key role of Lewis acid sites in aldol condensation of acetaldehyde over ZrO_2–SiO_2 catalyst [**63**]. However, it is noteworthy that all catalysts presented in this study perform significantly worse than Zr-containing zeolites [**64**]. While $NHSG$-prepared catalysts reached a maximum 1.6 % benzalacetone

yield after 4 h, the $Zr-BEA$ zeolite exhibited 94 % conversion with 98 % selectivity to benzalacetone after 5 h [**64**].

The results clearly show the importance of Lewis acidity in both MPV redox reaction and aldol condensation in agreement with the literature [**23,52,62-64**]. Activities in both reactions followed the Lewis acid site numbers. Importantly, the Lewis acid site numbers were governed by the Zr dispersion in zirconosilicates: materials prepared by $NHSG$ exhibited better Zr dispersion and catalytic activity than the catalyst prepared by dry impregnation.

Noteworthy, MPV redox reaction and aldol condensation reaction are the key steps of the ETB process [**4**]. However, both individual reactions were performed under different conditions (low temperature, liquid phase, batch) and applying different substrates. Therefore, the results must be compared and considered carefully when studying the ethanol-acetaldehyde conversion to BD (see **Section 3.6**).

3.6. Ethanol-acetaldehyde mixture conversion to 1,3-butadiene

Zirconosilicates prepared by $NHSG$ ($\boldsymbol{NH-160}$ and $\boldsymbol{NH-140}$) were tested as catalysts for the gas-phase ethanol-acetaldehyde mixture (2.5:1 mol ratio) transformation to 1,3-butadiene at 255, 290, and 325 °C. The catalytic properties of $NHSG$-prepared materials were compared to the benchmark catalyst prepared by dry impregnation on $NHSG$ prepared support ($\boldsymbol{DI-140}$). The support for $\boldsymbol{DI-140}$ was prepared by $NHSG$ method to avoid significant porosity differences that would impair the fair comparison.

Ethanol-acetaldehyde mixture was used to skip the first step of the ethanol-to-butadiene transformation (**Scheme 1**, step 1) due to the absence of sites promoting ethanol dehydrogenation in our catalysts. Redox sites were omitted on purpose to focus on the reactions that take place on acid sites, namely aldol condensation, dehydration, and MPV redox reaction (**Scheme 1**, steps 2-5).

The major products of the catalytic reaction were butadiene and ethylene, accounting for $>$ 97 % of the selectivity. Ethylene was formed in a side reaction (direct dehydration of ethanol) [**65**]. Frequently, ethylene is the major by-product of ethanol to butadiene transformation over acid materials (e.g., metal silicates) [**18,41**]. Propene, all butene isomers, and diethyl ether were observed in negligible amounts. Carbon balances fluctuated in the 89- 107 % range (**Tables 1S** and **2S**).

The total conversion of the ethanol-acetaldehyde mixture decreased in the order $\boldsymbol{NH-140} > \boldsymbol{NH-160} > \boldsymbol{DI-140}$ at all temperatures and thus followed the Lewis acid site numbers (**Fig. 7**A), similar to other reports on catalysts based on Zr in silica [**16**]. Notably, this trend followed the results presented in Section 3.5 (MPV redox reaction and aldol condensation performed in batch). The influence of Zr dispersion homogeneity could be discerned: more homogeneous samples (prepared by $NHSG$) perform better. The highest conversion (78 %) was observed at 325 °C for $\boldsymbol{NH-140}$.

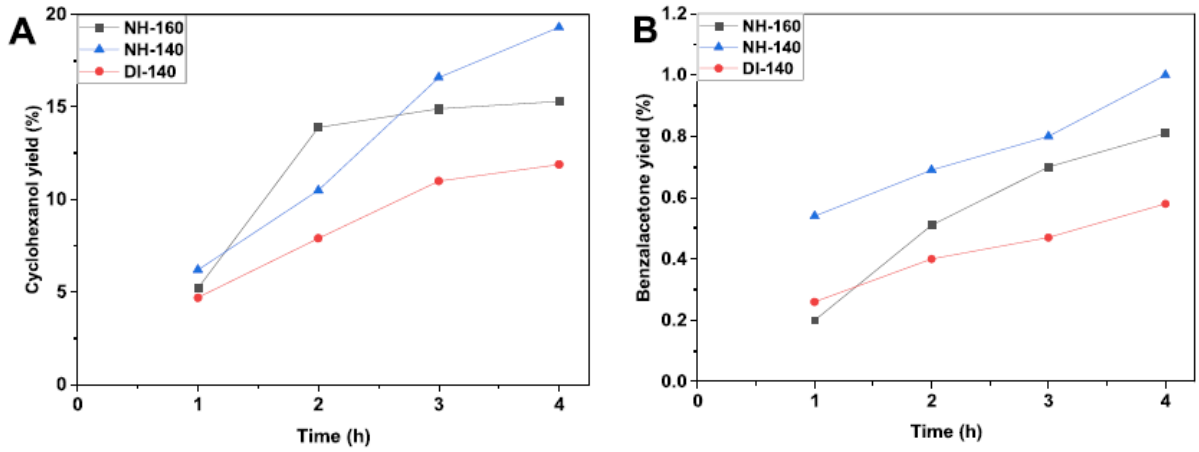

Fig. 6. Catalytic performance of zirconosilicate catalysts in MPV cyclohexanone reduction (A)

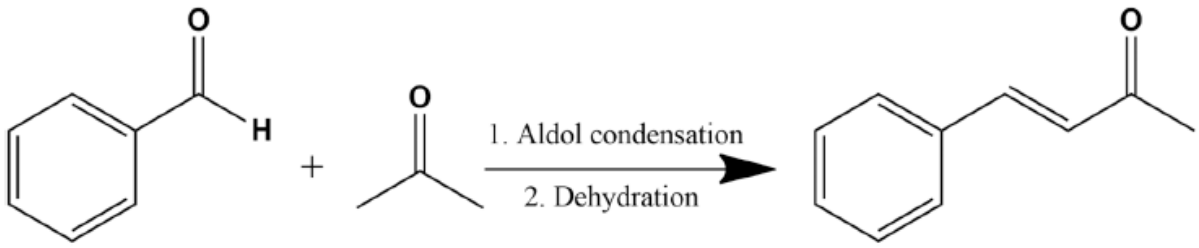

Scheme 4. Aldol condensation of benzaldehyde and acetone followed by dehydration providing benzalacetone as the final product.

Butadiene yields followed mostly the conversion patterns (**Fig. 7**B). However, the actual BD yield values were lower by 7-15 % compared to the respective conversion rates. This is due to the ethylene production, which accounted for 10-15 % yield at 325 °C (**Table 2S**). The most productive catalyst towards butadiene ($\boldsymbol{NH-140}$; 60 %, **Table 2S**) was also the most productive towards ethylene (15 %, **Table 2S**). Higher ethylene productivity over acid catalysts displaying higher activity in ETB process has already been described previously and explained by the higher amount of acid sites [**18,41**]. The highest number of Lewis acid sites in $\boldsymbol{NH-140}$ out of the studied catalysts is in good agreement with these results (**Table 3**). As the fraction of the acid sites preserved after desorption at 150 and 250 °C remained similar among the samples (**Table 3**), the number of stronger acid sites was higher in this sample in comparison to $\boldsymbol{NH-160}$ and $\boldsymbol{DI-140}$. Solid acids with stronger acid sites produced more ethylene than the weaker ones [**44,46**]. Therefore, it can be suggested that $\boldsymbol{NH-140}$ generated more ethylene due to the higher number of stronger acid sites.

The selectivity to BD was compared at 290 °C for NH-160 and NH-140 and at 325 °C for $\boldsymbol{DI-140}$ (similar conversion levels ranging from 59 % to 65 %; **Table 1S** and **2S**). The highest selectivity was exhibited by $\boldsymbol{DI-140}$ (89 %), closely followed by NH-140 (87 %). $\boldsymbol{NH-160}$ displayed somewhat lower BD selectivity (74 % at 290 °C). This was reflected in the butadiene yields (**Fig. 7**B), where $\boldsymbol{DI-140}$ outperformed $\boldsymbol{NH-160}$ at lower temperatures.

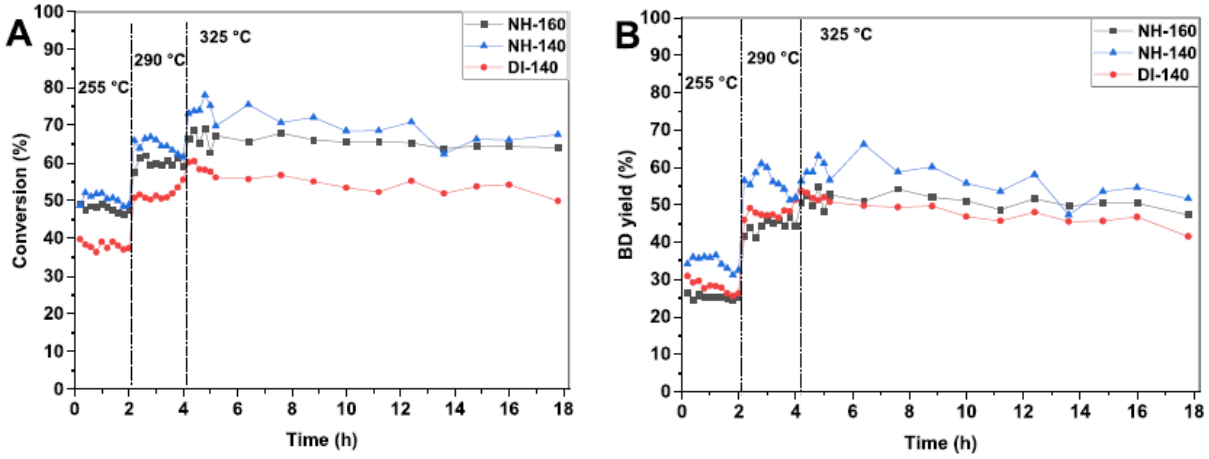

Fig. 7. Ethanol-acetaldehyde conversion (A) and butadiene yield (B) of zirconosilicate samples during catalytic tests.

The values of conversion (75 %), butadiene selectivity (80 %), and butadiene productivity (0.39 g g^{-1} h^{-1}) exhibited by $\boldsymbol{NH-140}$ at 325 °C compare well and often outperform other catalysts applied in the ethanol-acetaldehyde conversion to BD and ETB process at similar temperatures (**Table 4**). The $WHSV$ (0.65 g h^{-1}) to achieve these promising results was rather low, comparable to catalysts based on zeolites, including $Ta-BEA$ and both pure and hierarchical $Zr-BEA$ catalysts [**17,25,28,29,66**].

Table 4 Catalytic performance of related materials in the ethanol-acetaldehyde conversion to BD and ETB process. Catalysts without dehydrogenation promoter using ethanol-acetaldehyde mixtures as feedstock are reported in the first part of the table. Catalysts with dehydrogenation promoter (Cu, Ag, Zn) using pure ethanol as a feedstock are shown in the second part of the table.

Catalyst	WHSV (g g^{-1} h^{-1})	Temperature (°C)	Conversion (%)	BD selectivity (%)	BD productivity (g g^{-1} h^{-1})	Reference
NH-140	0.65	325	75	80	0.39	This work
Zr-BEA	1.04	325	58	70	0.42	[25]
Zr-BEA hierarchical	1.04	325	58	75	0.45	[25]
Zr-BEA+mesopores	1.0	325	56	66	0.37	[66]
ZrO_2/NanoSiO_2	1.8	320	59	93	0.99	[20]
ZrO_2-SiO_2 HSG	1.8	320	45	70	0.57	[19]
Ta_2O_5-SiO_2	1[a]	350	47	80	-	[15]
Ta-BEA	0.8	325	44	87	0.31	[28]
Cu-Ta-BEA	0.5	325	88	73	0.32	[29]
Ag-Zr-BEA	0.64	320	30	64	0.12	[17]
Ag-ZrO_2-SiO_2	0.45	325	86	69	0.27	[18]
Zn-Ta-TUD	5.3	400	94	73	3.64	[26]

[a] *$LHSV$ (h^{-1}).*

The reason for this similar behavior might be a significant microporosity in all micro-mesoporous zirconosilicates presented herein; catalysts with more open porosity might achieve significantly higher BD productivities [**20,26**]. Strikingly, the $Zr-BEA$ zeolites showed much better results in MPV redox reaction and aldol condensation performed in liquid phase (see **Section 3.5**) [**52,64**], but the $Zr-BEA$ zeolites exhibited rather similar catalytic performance in butadiene production from ethanol-acetaldehyde mixtures to $NHSG$-prepared catalysts presented herein (**Table 4**).

As catalyst deactivation presents a major issue for the targeted application, the catalytic tests at 325 °C were continued for 14 h TOS to assess the stability of the catalysts (**Fig. 7**). Both conversion and BD yield tended to decrease slowly (from -3 % to -9 % drop after 14 h, **Table 3S**) for all studied catalysts.

The sample $\boldsymbol{DH-160}$ was the most stable: its conversion decreased from ~50 % to ~47 % only (**Table 3S**). The samples prepared at 140 °C lost slightly more catalytic activity. The reason for these subtle differences might be both in different porosity properties and/or lower conversion rates exhibited by $\boldsymbol{DH-160}$. BD selectivity was stable for all three studied catalysts during 14 h TOS.

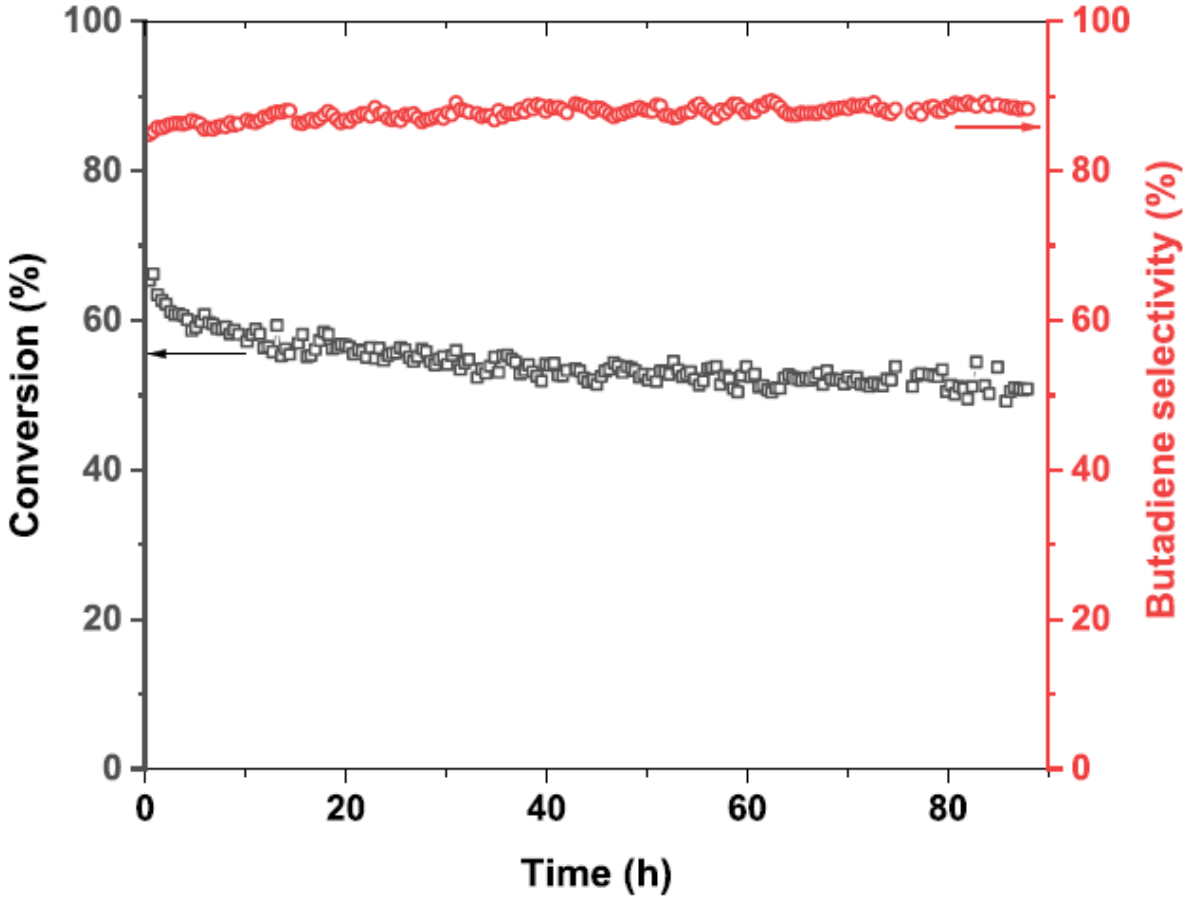

Fig. 8. Conversion and butadiene selectivity of sample $NH-140$ during catalytic stability test (325 °C, 90 h, $WHSV$ = 0.65 g g 1 h 1).

The catalytic stability of the most active and BD-productive sample ($\boldsymbol{NH-140}$) was additionally studied for 90 h at 325 °C applying the same $WHSV$ (0.65 g g^{-1} h^{-1}; **Fig. 8**). In a good agreement with preliminary stability tests (14 h, **Fig. 7**, see above) the butadiene selectivity was stable, while conversion decreased in time. The extended experiment time revealed that the conversion deterioration takes place mainly during first 20 h of the catalytic reaction (~12 % conversion loss), while a slower deactivation rate was observed during additional 70 h of experiment (~5 % conversion loss).

The slow deactivation trend with stable selectivity to BD was also observed for tantalum oxide supported on mesoporous silica [**15**]. On the contrary, the stability of $Zr-BEA$ zeolite has been reported to achieve poor results. Microporous $Zr-BEA$ lost ~22 % ethanol/acetaldehyde conversion during 6 h TOS at 325 °C. The deterioration rate was improved in the case of hierarchical $Zr-BEA$. The best material lost 14 % conversion under identical conditions [**25**]. Similarly, the $Zr-BEA$ zeolite containing mesopores and high Zr loading lost ~28 % conversion after 100 h TOS, while selectivity to butadiene was stable [**66**]. The activity losses reported for both fully microporous and hierarchical

$Zr-BEA$ zeolites are significantly worse than for micro-mesoporous zirconosilicates presented herein highlighting the decisive advantage of $NHSG$ synthetic approach.

4. Conclusions

In this study, we have broadened our previous work on nonhydrolytic sol-gel condensation between silicon tetraacetate and zirconium tetrakis(diethylamide) in 1:1 molar ratio [**38**]. The reaction conditions enabling reaching the $Si{:}\,Zr$ molar ratio 64:1 have been discerned: autoclave, 140/160 °C. It has been found that Pluronic F127 is not stable at 160 °C in the presence of zirconium and decomposes. As a result, zirconosilicate NH-160 prepared at 160 °C exhibited a broad pore size distribution. On the other hand, the application of silicon tetrachloride enabled to obtain gels at lower temperature (140 °C), preserve Pluronic F127, and obtain, after calcination, micro-mesoporous products (17-26 % micropore volume) with a hysteresis in medium pressure range in their isotherms and pore size maxima of 3.7 nm.

The structure of $NHSG$-prepared zirconosilicates was described by IR, $DRUV-Vis$, XPS, and NMR spectroscopy, $STEM-EDS$, and XRD and compared to the benchmark sample prepared by dry impregnation on support with similar porosity ($NHSG$-prepared). It has been shown that $NHSG$ condensation provides materials with a better zirconium dispersion in the silica matrix than the conventional dry impregnation technique. This was reflected in the number of Lewis acid sites (estimated by IR spectroscopy combined with pyridine adsorption). The $NHSG$-prepared zirconosilicates contained up to double the number of Lewis acid sites present in the benchmark sample prepared by dry impregnation.

The studied zirconosilicates were applied as heterogeneous catalysts in ethanol-acetaldehyde conversion to butadiene, MPV reduction of cyclohexanone with isopropanol, and aldol cross-condensation of benzaldehyde with acetone. The activity of zirconosilicate catalysts in all three reactions followed the Lewis acid site numbers and in ethanol-acetaldehyde conversion to butadiene was comparable to $Zr-BEA$-based catalysts. Selectivity to butadiene was high for all materials (76-90 % at 325 °C). The best catalyst (mostly mesoporous zirconosilicate prepared by non-hydrolytic sol-gel, $\boldsymbol{NH-140}$) displayed an average 75 % ethanol-acetaldehyde conversion with 80 % butadiene selectivity at 325 °C ($WHSV = 0.65$ h^{-1}). The micro-mesoporous zirconosilicate materials reported herein showed improved stability in ethanol-acetaldehyde conversion in comparison to $Zr-BEA$-based materials. Selectivity to butadiene was stable during both preliminary (14 h) and extended (90 h) stability test; conversion decreased by 12 % after first 20 h TOS and by 5 % after additional 70 h TOS.

References

[1] S. Lebedev, British patent, 331402, 1929.

[2] B.B. Corson, H.E. Jones, C.E. Welling, J.A. Hinckley, E.E. Stahly, Butadiene from ethyl alcohol. catalysis in the one-and two-stop processes, Ind. Eng. Chem. 42 (1950) 359-373, **https://doi.org/10.1021/ie50482a039**.

[3] G. Pomalaza, M. Capron, V. Ordomsky, F. Dumeignil, Recent breakthroughs in the conversion of ethanol to butadiene, Catalysts 6 (2016) 203, **https://doi.org/ 10.3390/catal6120203**.

[4] C. Angelici, B.M. Weckhuysen, P.C.A. Bruijnincx, Chemocatalytic conversion of ethanol into butadiene and other bulk chemicals, ChemSusChem 6 (2013) 1595-1614, **https://doi.org/10.1002/cssc.201300214**.

[5] D. Cespi, F. Passarini, I. Vassura, F. Cavani, Butadiene from biomass, a life cycle perspective to address sustainability in the chemical industry, Green Chem. 18 (2016) 1625-1638, **https://doi.org/10.1039/C5GC02148K**.

[6] I. Bin Samsudin, H. Zhang, S. Jaenicke, G.K. Chuah, Recent advances in catalysts for the conversion of ethanol to butadiene, Chem. - Asian J. 15 (2020) 4199-4214, **https://doi.org/10.1002/ASIA.202001023**.

[7] P.I. Kyriienko, O.V. Larina, S.O. Soloviev, S.M. Orlyk, Catalytic conversion of ethanol into 1,3-butadiene: achievements and prospects: a review, Theor. Exp. Chem. 56 (2020), **https://doi.org/10.1007/s11237-020-09654-2**.

[8] W.M. Quattlebaum, W.J. Toussaint, J.T. Dunn, Deoxygenation of certain aldehydes and ketones: preparation of butadiene and styrene, J. Am. Chem. Soc. 69 (1947) 593-599, **https://doi.org/10.1021/JA01195A040/ASSET/JA01195A040.FP.PNG_ V03**.

[9] P. Müller, S.P. Burt, A.M. Love, W.P. McDermott, P. Wolf, I. Hermans, Mechanistic study on the lewis acid catalyzed synthesis of 1,3-butadiene over Ta-BEA using modulated operando DRIFTS-MS, ACS Catal. 6 (2016) 6823-6832, **https://doi.org/ 10.1021/acscatal.6b01642**.

[10] D. Dussol, N. Cadran, N. Laloue, L. Renaudot, J.M. Schweitzer, New insights of butadiene production from ethanol: elucidation of concurrent reaction pathways and kinetic study, Chem. Eng. J. 391 (2020), **https://doi.org/10.1016/J.CEJ.2019.123586**.

[11] C. Angelici, M.E.Z. Velthoen, B.M. Weckhuysen, P.C.A. Bruijnincx, Influence of acid-base properties on the Lebedev ethanol-to-butadiene process catalyzed by SiO2 -MgO materials, Catal. Sci. Technol. 5 (2015) 2869-2879, **https://doi.org/ 10.1039/C5CY00200A**.

[12] C. Angelici, F. Meirer, A.M.J. Van Der Eerden, H.L. Schaink, A. Goryachev, J. P. Hofmann, E.J.M. Hensen, B.M. Weckhuysen, P.C.A. Bruijnincx, Ex situ and operando studies on the role of copper in Cu-promoted SiO2-MgO catalysts for the lebedev ethanol-to-butadiene process, ACS Catal. 5 (2015) 6005-6015, **https://doi. org/10.1021/acscatal.5b00755**.

[13] E.V. Makshina, W. Janssens, B.F. Sels, P.A. Jacobs, Catalytic study of the conversion of ethanol into 1,3-butadiene, Catal. Today 198 (2012) 338-344, **https://doi.org/10.1016/j.cattod.2012.05.031**.

[14] V.L. Sushkevich, I.I. Ivanova, V.V. Ordomsky, E. Taarning, Design of a metal-promoted oxide catalyst for the selective synthesis of butadiene from ethanol, ChemSusChem 7 (2014) 2527-2536, **https://doi.org/10.1002/cssc.201402346**.

[15] S.-Y. Jeong, T.-W. Kim, C.-U. Kim, H.-J. Chae, H.-K. Kim, K.-E. Jeong, Y.-K. Moon, Butadiene production from bioethanol and acetaldehyde over tantalum oxide-supported ordered mesoporous silica catalysts, Appl. Catal. B Environ. 150-151 (2013) 596-604, **https://doi.org/10.1016/j.apcatb.2013.12.023**.

[16] V.L. Sushkevich, I.I. Ivanova, E. Taarning, Ethanol conversion into butadiene over Zr-containing molecular sieves doped with silver, Green Chem. 17 (2015) 2552-2559, **https://doi.org/10.1039/C4GC02202E**.

[17] V.L. Sushkevich, I.I. Ivanova, Ag-promoted ZrBEA zeolites obtained by postsynthetic modification for conversion of ethanol to butadiene, ChemSusChem 9 (2016) 2216-2225, **https://doi.org/10.1002/cssc.201600572**.

[18] V.L. Dagle, M.D. Flake, T.L. Lemmon, J.S. Lopez, L. Kovarik, R.A. Dagle, Effect of the SiO2 support on the catalytic performance of Ag/ZrO2/SiO2 catalysts for the single-bed production of butadiene from ethanol, Appl. Catal. B Environ. 236 (2018) 576-587, **https://doi.org/10.10Wj.apcatb.2018.05.055**.

[19] Z. Han, X. Li, M. Zhang, Z. Liu, M. Gao, Sol-gel synthesis of ZrO 2 -SiO 2 catalysts for the transformation of bioethanol and acetaldehyde into 1,3-butadiene, RSC Adv. 5 (2015) 103982-103988, **https://doi.org/10.1039/C5RA22623F**.

[20] M. Gao, H. Jiang, M. Zhang, The influence of calcination temperatures on the acid-based properties and catalytic activity for the 1,3-butadiene synthesis from ethanol/acetaldehyde mixture, Appl. Surf. Sci. 439 (2018) 1072-1078, **https://doi. org/10.1016/j.apsusc.2018.01.053**.

[21] V.L. Sushkevich, D. Palagin, I.I. Ivanova, With open arms: open sites of ZrBEA zeolite facilitate selective synthesis of butadiene from ethanol, ACS Catal. 5 (2015) 4833-4836, **https://doi.org/10.1021/acscatal.5b01024**.

[22] V.L. Sushkevich, A. Vimont, A. Travert, I.I. Ivanova, Spectroscopic evidence for open and closed lewis acid sites in ZrBEA zeolites, J. Phys. Chem. C 119 (2015) 17633-17639, **https://doi.org/10.1021/acs.jpcc.5b02745**.

[23] V.L. Sushkevich, I.I. Ivanova, S. Tolborg, E. Taarning, Meerwein-Ponndorf-Verley-Oppenauer reaction of crotonaldehyde with ethanol over Zr-containing catalysts, J. Catal. 316 (2014) 121-129, **https://doi.org/10.1016/j-jcat.2014.04.019**.

[24] P.A. Kots, A.V. Zabilska, I.I. Ivanova, Selective self-condensation of butanal over Zr-BEA zeolites, ChemCatChem 12 (2020) 248-258, **https://doi.org/10.1002/ CCTC.201901556**.

[25] G. Yang, L. Wang, H. Jiang, Preparation of p zeolite with intracrystalline mesoporosity via surfactant -templating strategy and its application in ethanol-acetaldehyde to butadiene, Microporous Mesoporous Mater. 316 (2021), **https:// doi.org/10.1016/J.MICROMESO.2021.110949**.

[26] G. Pomalaza, G. Vofo, M. Capron, F. Dumeignil, ZnTa-TUD-1 as an easily prepared, highly efficient catalyst for the selective conversion of ethanol to 1,3-butadiene, Green. Chem. 20 (2018) 3203-3209, **https://doi.org/10.1039/C8GC01211C**.

[27] G. Pomalaza, P. Simon, A. Addad, M. Capron, F. Dumeignil, Properties and activity of Zn-Ta-TUD-1 in the Lebedev process, Green. Chem. 22 (2020) 2558-2574, **https://doi.org/10.1039/D0GC00103A**.

[28] P.I. Kyriienko, O.V. Larina, S.O. Soloviev, S.M. Orlyk, S. Dzwigaj, High selectivity of TaSiBEA zeolite catalysts in 1,3-butadiene production from ethanol and acetaldehyde mixture, Catal. Commun. 77 (2016) 123-126, **https://doi.org/ 10.1016/j.catcom.2016.01.023**.

[29] P.I. Kyriienko, O.V. Larina, S.O. Soloviev, S.M. Orlyk, C. Calers, S. Dzwigaj, Ethanol Conversion into 1,3-Butadiene by the Lebedev Method over MTaSiBEA Zeolites (M = Ag, Cu, Zn), ACS Sustain. Chem. Eng. 5 (2017) 2075-2083, **https://doi.org/ 10.1021/acssuschemeng.6b01728**.

[30] W. Dai, S. Zhang, Z. Yu, T. Yan, G. Wu, N. Guan, L. Li, Zeolite structural confinement effects enhance one-pot catalytic conversion of ethanol to butadiene, ACS Catal. 7 (2017) 3703-3706, **https://doi.org/10.1021/acscatal.7b00433**.

[31] L. Qi, Y. Zhang, M.A. Conrad, C.K. Russell, J. Miller, A.T. Bell, Ethanol conversion to butadiene over isolated zinc and yttrium sites grafted onto dealuminated beta zeolite, J. Am. Chem. Soc. 142 (2020) 14674-14687, **https://doi.org/10.1021/ jacs.0c06906**.

[32] A. Styskalik, D. Skoda, C. Barnes, J. Pinkas, The power of non-hydrolytic sol-gel chemistry: a review, Catalysts 7 (2017) 168-210, **https://doi.org/10.3390/ catal7060168**.

[33] D.P. Debecker, V. Hulea, P.H. Mutin, Mesoporous mixed oxide catalysts via nonhydrolytic sol-gel: a review, Appl. Catal., A. 451 (2013) 192-206, **https://doi.org/ 10.1016/j.apcata.2012.11.002**.

[34] D.P. Debecker, P.H. Mutin, Non-hydrolytic sol-gel routes to heterogeneous catalysts, Chem. Soc. Rev. 41 (2012) 3624-3650, **https://doi.org/10.1039/C2CS15330K**.

[35] D. Skoda, B. Hanulikova, A. Styskalik, V. Vykoukal, P. Machac, P. Urbanek, E. Domincova Bergerova, L. Simonikova, I. Kuritka, Non-aqueous synthesis of homogeneous molybdenum silicate microspheres and their application as heterogeneous catalysts in olefin epoxidation and selective aniline oxidation, J. Ind. Eng. Chem. 107 (2022) 320-332, **https://doi.org/10.1016/j. jiec.2021.12.001**.

[36] A.A. Bernardes, G.L. Scheffler, C. Radtke, D. Pozebon, J.H.Z. dos Santos, Z.N. da Rocha, Supported metallocenes produced by a non-hydrolytic sol-gel process: application in ethylene polymerization, Colloids Surf. A Physicochem. Eng. Asp. 584 (2020), 124020, **https://doi.org/10.1016/j.colsurfa.2019.124020**.

[37] L.B. Capeletti, M. do Carmo Martins Alves, M.B. Cardoso, J.H.Z. dos Santos, Hybrid silica based catalysts prepared by the encapsulation of zirconocene compound via non-hydrolytic sol-gel method for ethylene polymerization, Appl. Catal. A Gen. 560 (2018) 225-235, **https://doi.org/10.1016/j.apcata.2018.03.013**.

[38] D. Skoda, A. Styskalik, Z. Moravec, P. Bezdicka, J. Pinkas, Templated nonhydrolytic synthesis of mesoporous zirconium silicates and their catalytic properties, J. Mater. Sci. 50 (2015) 3371-3382, **https://doi.org/10.1007/s10853-015-8888-1**.

[39] D. Skoda, A. Styskalik, Z. Moravec, P. Bezdicka, C.E. Barnes, J. Pinkas, Mesoporous titanosilicates by templated non-hydrolytic sol-gel reactions, J. Sol-Gel Sci. Technol. 74 (2015) 810-822, **https://doi.org/10.1007/s10971-015-3666-8**.

[40] A. Styskalik, D. Skoda, J. Pinkas, S. Mathur, Non-hydrolytic synthesis of titanosilicate xerogels by acetamide elimination and their use as epoxidation catalysts, J. Sol-Gel Sci. Technol. 63 (2012) 463-472, **https://doi.org/10.1007/ s10971-012-2808-5**.

[41] D.D. Dochain, A. Styskalik, D.P. Debecker, Ag- and Cu-promoted mesoporous Ta-SiO2 catalysts prepared by non-hydrolytic sol-gel for the conversion of ethanol to butadiene, Catalysts 9 (2019) 920, **https://doi.org/10.3390/catal9110920**.

[42] P.H. Mutin, A. Vioux, Nonhydrolytic processing of oxide-based materials: simple routes to control homogeneity, morphology, and nanostructure, Chem. Mater. 21 (2009) 582-596, **https://doi.org/10.1021/cm802348c**.

[43] L. Bourget, R.J.P. Corriu, D. Leclercq, P.H. Mutin, A. Vioux, Non-hydrolytic sol-gel routes to silica, J. Non Cryst. Solids 242 (1998) 81-91, **https://doi.org/10.1016/ S0022-3093(98)00789-3**.

[44] A. Styskalik, I. Kordoghli, C. Poleunis, A. Delcorte, Z. Moravec, L. Simonikova, V. Kanicky, C. Aprile, L. Fusaro, D.P. Debecker, Hybrid mesoporous aluminosilicate catalysts obtained by non-hydrolytic sol-gel for ethanol dehydration, J. Mater. Chem. A 8 (2020) 23526-23542, **https://doi.org/10.1039/d0ta07016e**.

[45] D. Skoda, A. Styskalik, Z. Moravec, P. Bezdicka, J. Bursik, P.H. Mutin, J. Pinkas, Mesoporous SnO 2 -SiO 2 and Sn-silica-carbon nanocomposites by novel nonhydrolytic templated sol-gel synthesis, RSC Adv. 6 (2016) 68739-68747, **https:// doi.org/10.1039/C6RA16556G**.

[46] A. Styskalik, V. Vykoukal, L. Fusaro, C. Aprile, D.P. Debecker, Mildly acidic aluminosilicate catalysts for stable performance in ethanol dehydration, Appl. Catal. B Environ. (2020), 118926, **https://doi.org/10.1016/j.apcatb.2020.118926**.

[47] J.A. Navío, M. Macías, G. Colon, P.J. Sánchez-Soto, V. Augugliaro, L. Palmisano, Combined use of XPS, IR and EDAX techniques for the characterization of ZrO2-SiO2 powders prepared by a sol-gel process, Appl. Surf. Sci. 81 (1994) 325-329, **https://doi.org/10.1016/0169-4332(94)90289-5**.

[48] R. Kore, R. Srivastava, B. Satpati, Highly efficient nanocrystalline zirconosilicate catalysts for the aminolysis, alcoholysis, and hydroamination reactions, ACS Catal. 3 (2013) 2891-2904, **https://doi.org/10.1021/cs400732f**.

[49] M. Andrianainarivelo, R. Corriu, D. Leclercq, P.H. Mutin, A. Vioux, Mixed oxides SiO2-ZrO2 and SiO2-TiO2 by a non-hydrolytic sol-gel route, J. Mater. Chem. 6 (1996) 1665-1671, **https://doi.org/10.1039/JM9960601665**.

[50] S.W. Lee, R.A. Condrate, The infrared and Raman spectra of ZrO2-SiO2 glasses prepared by a sol-gel process, J. Mater. Sci. 23 (1988) 2951-2959, **https://doi.org/ 10.1007/BF00547474**.

[51] R. Jerome, P. Teyssie, J.J. Pireaux, J.J. Verbist, Surface analysis of polymers end-capped with metal carboxylates using x-ray photoelectron spectroscopy, Appl. Surf. Sci. 27 (1986) 93-105, **https://doi.org/10.1016/0169-4332(86)90098-X**.

[52] Y. Zhu, G. Chuah, S. Jaenicke, Chemo- and regioselective Meerwein-Ponndorf-Verley and Oppenauer reactions catalyzed by Al-free Zr-zeolite beta, J. Catal. 227 (2004) 1-10, **https://doi.org/10.1016/JJCAT.2004.05.037**.

[53] A.P. Dementjev, O.P. Ivanova, L.A. Vasilyev, A.V. Naumkin, D.M. Nemirovsky, D. Y. Shalaev, Altered layer as sensitive initial chemical state indicator*, J. Vac. Sci. Technol. A Vac., Surf., Film. 12 (1994) 423-427, **https://doi.org/10.1116/ 1.579258**.

[54] Y. Hasegawa, A. Ayame, Investigation of oxidation states of titanium in titanium silicalite-1 by X-ray photoelectron spectroscopy, Catal. Today 71 (2001) 177-187, **https://doi.org/10.1016/S0920-5861(01)00428-X**.

[55] W. Thitsartarn, S. Kawi, Transesterification of Oil by Sulfated Zr-Supported Mesoporous Silica, Ind. Eng. Chem. Res. 50 (2011) 7857-7865, **https://doi.org/ 10.1021/ie1022817**.

[56] B.L. Newalkar, J. Olanrewaju, S. Komarneni, Microwave-hydrothermal synthesis and characterization of zirconium substituted SBA-15 mesoporous silica, J. Phys. Chem. B. 105 (2001) 8356-8360, **https://doi.org/10.1021/jp010889l**.

[57] A. Zheng, S.-J. Huang, S.-B. Liu, F. Deng, Acid properties of solid acid catalysts characterized by solid-state 31P NMR of adsorbed phosphorous probe molecules, Phys. Chem. Chem. Phys. 13 (2011) 14889, **https://doi.org/10.1039/c1cp20417c**.

[58] A. Styskalik, J.G. Abbott, M.C. Orick, D.P. Debecker, C.E. Barnes, Synthesis, characterization and catalytic activity of single site, Lewis acidic aluminosilicates, Catal. Today 334 (2019) 131-139, **https://doi.org/10.1016/j.cattod.2018.11.079**.

[59] J.D. Lewis, M. Ha, H. Luo, A. Faucher, V.K. Michaelis, Y. Román-Leshkov, Distinguishing active site identity in Sn-beta zeolites using 31 P MAS NMR of adsorbed trimethylphosphine oxide, ACS Catal. 8 (2018) 3076-3086, **https://doi. org/10.1021/acscatal.7b03533**.

[60] C.A. Emeis, Determination of integrated molar extinction coefficients for infrared absorption bands of pyridine adsorbed on solid acid catalysts, J. Catal. 141 (1993) 347-354.

[61] E.J.M. Hensen, D.G. Poduval, D.A.J.M. Ligthart, J.A.R. Van Veen, M.S. Rigutto, Quantification of strong br0nsted acid sites in aluminosilicates, J. Phys. Chem. C 114 (2010) 8363-8374, **https://doi.org/10.1021/jp9106348**.

[62] G. Li, W.H. Fu, Y.M. Wang, Meerwein-Ponndorf-Verley reduction of cyclohexanone catalyzed by partially crystalline zirconosilicate, Catal. Commun. 62 (2015) 10-13, **https://doi.org/10.1016ZJ.CATCOM.2014.12.016**.

[63] V.V. Ordomsky, V.L. Sushkevich, I.I. Ivanova, Study of acetaldehyde condensation chemistry over magnesia and zirconia supported on silica, J. Mol. Catal. A Chem. 333 (2010) 85-93, **https://doi.org/10.1016/J.M0LCATA.2010.10.001**.

[64] J.D. Lewis, S. Van De Vyver, Y. Romaán-Leshkov, Acid-base pairs in lewis acidic zeolites promote direct aldol reactions by soft enolization, Angew. Chem. Int. Ed. 54 (2015) 9835-9838, **https://doi.org/10.1002/ANIE.201502939**.

[65] T.K. Phung, L. Proietti Hernáandez, A. Lagazzo, G. Busca, Dehydration of ethanol over zeolites, silica alumina and alumina: Lewis acidity, Br0nsted acidity and confinement effects, Appl. Catal. A Gen. 493 (2015) 77-89, **https://doi.org/ 10.1016/j.apcata.2014.12.047**.

[66] H. Jiang, L. Yi, G. Yang, L. Wang, Heteroatom zeolites with a high content of framework metal sites as Lewis-acid catalysts for the conversion of ethanol-acetaldehyde to 1,3-butadiene, Catal. Sci. Technol. (2023), **https://doi. org/10.1039/D2CY01841A**.